Open Journal of Metal, 2014, 4, 120-130
Published Online December 2014 in SciRes. http://www.scirp.org/journal/ojmetal
http://dx.doi.org/10.4236/ojmetal.2014.44014

Scientific Research

Theoretical and Numerical Study of Stress and Thermo-Optic in Photonic Crystal Fiber Laser in Different Pump Schemes

M. Abouricha[1*], A. Boulezhar[1], M. El Mouden[1,2], M. Kriraa[1], N. Rouchdi[1]

[1]Laboratory of Theoretical and Applied Physics, Faculty of Sciences-Ain Chok, Hassan II Casablanca University, Casablanca, Morocco
[2]Engineering Sciences Laboratory for Energy (LabSIPE), National School of Applied Sciences, El Jadida, Morocco
Email: *abourichamostafa@yahoo.fr

Received 9 October 2014; revised 6 November 2014; accepted 19 November 2014

Abstract

In this paper, we present a study of thermal, average power scaling, change in index of refraction and stress in photonic crystal fiber lasers with different pump schemes: forward pump scheme, backward pump scheme, forward pump scheme with reflection of 98%, backward pump scheme with reflection of 98% and bi-directional pump scheme. We show that management of thermal effects in fiber lasers will determine the efficiency and success of scaling-up efforts. In addition, we show that the most suitable scheme is the bi-directional.

Keywords

Pump Schemes, PCF Lasers Birefringence in Fiber Lasers, Diode-Pumped Fiber Lasers, Fiber Lasers, Scaling of Fiber Lasers, Yb-Doped Fiber Lasers, Thermal Effects in Fiber Lasers

1. Introduction

The superiorities of the conventional solid-state and gas lasers make Yb^{3+} doped fibers lasers reported [1]-[4]. Recently a new type of the pump schemes with the high brightness semiconductor diode pump laser was studied [5]. And the new type of photonic crystal fibers (PCFs) is attracting increasing interests because of its unique properties such as endlessly single-mode guiding, freedom of dispersion characteristics, and large mode area [6] [7]. We also concentrate on PCFs in which a core doped with Yb^{3+} surrounded by a lower index cladding, which is, surrounded by an air-clad region, in turn, surrounded by a second lower index cladding index.

By analytical and numerical calculation and using the finite-difference method (FDM), we have determined

How to cite this paper: Abouricha, M., *et al.* (2014) Theoretical and Numerical Study of Stress and Thermo-Optic in Photonic Crystal Fiber Laser in Different Pump Schemes. *Open Journal of Metal*, **4**, 120-130.
http://dx.doi.org/10.4236/ojmetal.2014.44014

the expressions of temperature distribution in different regions of the photonic crystal fiber laser (PCF) along the axial and radial directions from the integration of the steady-state heat equation for an isotropic medium. Then we used the expressions previously derived for the temperatures in Regions I, II, III, and IV [8] in the results of the expressions for the stress components ($\sigma_r(r)$, $\sigma_\varphi(r)$, and $\sigma_z(r)$) and the change in the index of refraction in Regions I, II, III, and IV. The results are compared in different pump schemes for giving the design guidelines to ensure maximum heat dissipation and saving pump powers. The calculated stress values are very small in different pump schemes, and will consequently have a negligible effect upon the index of refraction.

The resulting gradients are still small as the corresponding stress values. As a consequence, we expect that changes in the index of refraction due to the stress-optic effect will be negligible in different pump schemes, and thermally induced birefringence will be absent in fiber lasers (in all cases of pumping), the stress component $\sigma_z(r)$ increases with the increase of the length the fiber in the cases (forward pump schemes) and decreases along the fiber laser in the cases (backward pump schemes). These values are between -0.4×10^{-6} kg/m^2 and -3.4×10^{-6} kg/m^2 in the four primer cases. Moreover, in the case bi-directional pump scheme, its value is between -0.8×10^{-6} kg/m^2 and -1.8×10^{-6} kg/m^2. And the values of the change in index of refraction increases in the cases of forward pump schemes and decreases in the cases of the backward pump schemes, along the fiber laser. For the bi-directional, its value is even smaller.

2. Average Temperature in PCF

As shown in **Figure 1**, a typical high power Yb^{3+}-doped double-clad PCF laser consists of an Yb^{3+}-doped double PCF with reflectors on both of the ends.

Figure 2 shows the heat flow mechanisms in fiber laser and the radial coordinate r and the tangential angle φ. The quantities a, b_1, b_2 and b are the core, inner cladding, air-clad and outer cladding radii, respectively.

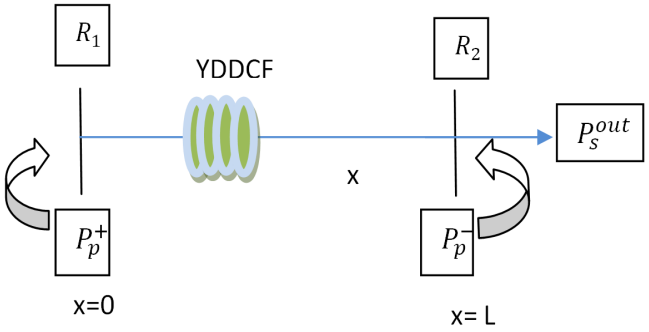

Figure 1. Schematic illustration of end pumped fiber lasers.

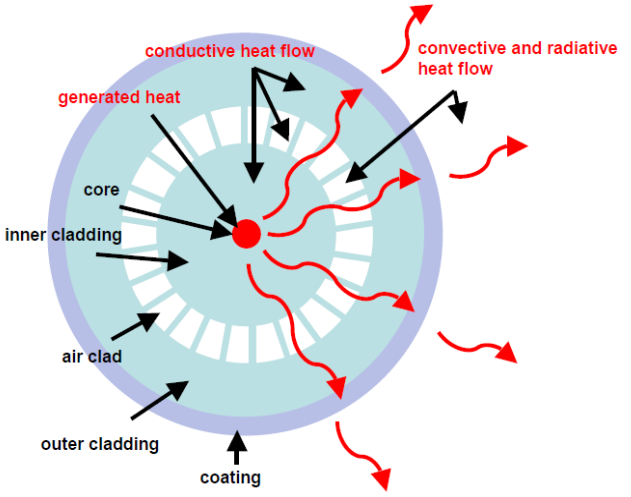

Figure 2. Heat flow mechanisms in PCF laser [9].

The temperature distribution in a fiber reported in [8] is necessary for determining the radially varying index of refraction due to $\mathrm{d}n/\mathrm{d}T$, the calculated stresses, and the change in index of refraction through the stress-optic effect.

We calculate the average temperature T_{av} as

$$T_{av} = \frac{\int_0^a T_1(r)\mathrm{d}r + \int_a^{b_1} T_2(r)\mathrm{d}r + \int_{b_1}^{b_2} T_3(r)\mathrm{d}r + \int_{b_2}^{b} T_4(r)\mathrm{d}r}{\int_0^b \mathrm{d}r} \tag{1}$$

where

$$\int_0^b \mathrm{d}r = b \tag{2}$$

$$\int_0^a T_1(r)\mathrm{d}r = T_0 a - \frac{Q(x)\times a^3}{12k_1} \tag{3}$$

$$\int_a^{b_1} T_2(r)\mathrm{d}r = T_1(a)(b_1 - a) + A(x)\times\left[b_1 \ln\left(\frac{b_1}{a}\right) - b_1 + a\right] \tag{4}$$

$$\int_{b_1}^{b_2} T_3(r)\mathrm{d}r = T_2(b_1)(b_2 - b_1) + B(x)\times\left[b_2 \ln\left(\frac{b_2}{b_1}\right) b_2 + b_1\right] \tag{5}$$

$$\int_{b_2}^{b} T_4(r)\mathrm{d}r = T_3(b_2)(b - b_2) + C(x)\times\left[b \ln\left(\frac{b}{b_2}\right) - b + b_2\right] \tag{6}$$

where the temperature expressions $T_1(r)$, $T_2(r)$, $T_3(r)$ and $T_4(r)$ are given by [8].

And

$$A(x) = -\frac{Q(x)a^2}{2k_1} \tag{7}$$

$$B(x) = \left[-\frac{Q(x)a^2}{2k_2} + \frac{\varepsilon\sigma b_1}{k_2}\left(T_c^4 - T_2(b_1)^4\right)\right] \tag{8}$$

$$C(x) = \left[\frac{k_2}{k_1}\left(-\frac{Q(x)a^2}{2k_2} + \frac{\varepsilon\sigma b_1}{k_2}\left(T_c^4 - T_2(b_1)^4\right)\right) - \frac{\varepsilon\sigma b_2}{k_1}\left(T_c^4 - T_3(b_2)^4\right)\right] \tag{9}$$

3. Stress Distributions

The length of the optical fibers is much greater than a typical fiber outside radius (b), we can invoke the plane-strain approximation [10] in which the z strain everywhere. The radial, tangential, and z stresses $\sigma_r(r)$, $\sigma_\varphi(r)$, and $\sigma_z(r)$ can be found from [11].

$$\sigma_r(r) = \frac{\alpha E}{(1-\vartheta)}\left[\frac{1}{b^2}\int_0^b T(r)r\mathrm{d}r - \frac{1}{r^2}\int_0^r T(r)r\mathrm{d}r\right] \tag{10}$$

$$\sigma_\varphi(r) = \frac{\alpha E}{(1-\vartheta)}\left[\frac{1}{b^2}\int_0^b T(r)r\mathrm{d}r - \frac{1}{r^2}\int_0^r T(r)r\mathrm{d}r - T(r)\right] \tag{11}$$

in the case where the fiber end faces are free of traction

$$\sigma_z(r) = \sigma_r(r) + \sigma_\varphi(r) \tag{12}$$

where α, E and v are thermal expansion coefficient, Young's modulus, and Poisson's ratio, respectively. Solution of (10)-(12), using the expressions previously derived for the temperatures in Regions I, II, III, and VI [8], results in the following final expressions for the stresses in Regions I, II, III, and IV:

$$\sigma_r^I(r)=\frac{\alpha E}{(1-\vartheta)}\left[\frac{1}{b^2}\left(\alpha(x)+\beta(x)+\gamma(x)+\delta(x)\right)-\frac{1}{r^2}\left(\alpha'(x)\right)\right] \tag{13}$$

$$\sigma_r^{II}(r)=\frac{\alpha E}{(1-\vartheta)}\left[\frac{1}{b^2}\left(\alpha(x)+\beta(x)+\gamma(x)+\delta(x)\right)-\frac{1}{r^2}\left(\alpha(x)+\beta'(x)\right)\right] \tag{14}$$

$$\sigma_r^{III}(r)=\frac{\alpha E}{(1-\vartheta)}\left[\frac{1}{b^2}\left(\alpha(x)+\beta(x)+\gamma(x)+\delta(x)\right)-\frac{1}{r^2}\left(\alpha(x)+\beta(x)+\gamma'(x)\right)\right] \tag{15}$$

$$\sigma_r^{IV}(r)=\frac{\alpha E}{(1-\vartheta)}\left[\frac{1}{b^2}\left(\alpha(x)+\beta(x)+\gamma(x)+\delta(x)\right)-\frac{1}{r^2}\left(\alpha(x)+\beta(x)+\gamma(x)+\delta'(x)\right)\right] \tag{16}$$

$$\sigma_\varphi^I(r)=\frac{\alpha E}{(1-\vartheta)}\left[\frac{1}{b^2}\left(\alpha(x)+\beta(x)+\gamma(x)+\delta(x)\right)+\frac{1}{r^2}\left(\alpha'(x)\right)-T_1(r)\right] \tag{17}$$

$$\sigma_\varphi^{II}(r)=\frac{\alpha E}{(1-\vartheta)}\left[\frac{1}{b^2}\left(\alpha(x)+\beta(x)+\gamma(x)+\delta(x)\right)+\frac{1}{r^2}\left(\alpha(x)+\beta'(x)\right)-T_2(r)\right] \tag{18}$$

$$\sigma_\varphi^{III}(r)=\frac{\alpha E}{(1-\vartheta)}\left[\frac{1}{b^2}\left(\alpha(x)+\beta(x)+\gamma(x)+\delta(x)\right)+\frac{1}{r^2}\left(\alpha(x)+\beta(x)+\gamma'(x)\right)-T_3(r)\right] \tag{19}$$

$$\sigma_\varphi^{IV}(r)=\frac{\alpha E}{(1-\vartheta)}\left[\frac{1}{b^2}\left(\alpha(x)+\beta(x)+\gamma(x)+\delta(x)\right)+\frac{1}{r^2}\left(\alpha(x)+\beta(x)+\gamma(x)+\delta'(x)\right)-T_4(r)\right] \tag{20}$$

$$\sigma_z^I(r)=\frac{\alpha E}{(1-\vartheta)}\left[\frac{2}{b^2}\left(\alpha(x)+\beta(x)+\gamma(x)+\delta(x)\right)-T_1(r)\right] \tag{21}$$

$$\sigma_z^{II}(r)=\frac{\alpha E}{(1-\vartheta)}\left[\frac{2}{b^2}\left(\alpha(x)+\beta(x)+\gamma(x)+\delta(x)\right)-T_2(r)\right] \tag{22}$$

$$\sigma_z^{III}(r)=\frac{\alpha E}{(1-\vartheta)}\left[\frac{2}{b^2}\left(\alpha(x)+\beta(x)+\gamma(x)+\delta(x)\right)-T_3(r)\right] \tag{23}$$

$$\sigma_Z^{IV}(r)=\frac{\alpha E}{(1-\vartheta)}\left[\frac{2}{b^2}\left(\alpha(x)+\beta(x)+\gamma(x)+\delta(x)\right)-T_4(r)\right] \tag{24}$$

where.

$$\alpha(x)=\int_0^a T_1(r)r\mathrm{d}r=T_0\frac{a^2}{2}-\frac{Q(x)a^4}{16k_1} \tag{25}$$

$$\beta(x)=\int_a^{b_1} T_2(r)r\mathrm{d}r=T_1(a)\left(\frac{b_1^2-a^2}{2}\right)+A(x)\left[\frac{b_1^2}{2}\ln\left(\frac{b_1}{a}\right)-\frac{b_1^2}{4}+\frac{a^2}{4}\right] \tag{26}$$

$$\gamma(x)=\int_{b_1}^{b_2} T_3(r)r\mathrm{d}r=T_2(b_1)\left(\frac{b_2^2-b_1^2}{2}\right)+B(x)\left[\frac{b_2^2}{2}\ln\left(\frac{b_2}{b_1}\right)-\frac{b_2^2}{4}+\frac{b_1^2}{4}\right] \tag{27}$$

$$\delta(x)=\int_{b_2}^{b} T_4(r)r\mathrm{d}r=T_3(b_2)\left(\frac{b^2-b_2^2}{2}\right)+C(x)\left[\frac{b^2}{2}\ln\left(\frac{b}{b_2}\right)-\frac{b^2}{4}+\frac{b_2^2}{4}\right] \tag{28}$$

$$\alpha'(x)=\int_0^r T_1(r)r\mathrm{d}r=T_0\frac{r^2}{2}-\frac{Q(x)r^4}{16k_1} \tag{29}$$

$$\beta'(x)=\int_a^r T_2(r)r\mathrm{d}r=T_1(a)\left(\frac{r^2-a^2}{2}\right)+A(x)\left[\frac{r^2}{2}\ln\left(\frac{r}{a}\right)-\frac{r^2}{4}+\frac{a^2}{4}\right] \tag{30}$$

$$\gamma'(x)=\int_{b_1}^{r}T_3(r)r\mathrm{d}r=T_2(b_1)\left(\frac{r^2-b_1^2}{2}\right)+B(x)\left[\frac{r^2}{2}\ln\left(\frac{r}{b_1}\right)-\frac{r^2}{4}+\frac{b_1^2}{4}\right] \tag{31}$$

$$\delta'(x)=\int_{b_2}^{r}T_4(r)r\mathrm{d}r=T_3(b_2)\left(\frac{r^2-b_2^2}{2}\right)+C(x)\left[\frac{r^2}{2}\ln\left(\frac{r}{b_2}\right)-\frac{r^2}{4}+\frac{b_2^2}{4}\right] \tag{32}$$

It can be shown that (13)-(24) satisfy the boundary conditions $\sigma_r^{IV}(r=b)=0$, $\sigma_r^{I}(r=0)=\sigma_r^{I}(r=0)$, $\sigma_\varphi^{IV}(r=b)=\sigma_z^{IV}(r=b)$, and the continuity conditions $\sigma_r^{I}(r=a)=\sigma_r^{II}(r=a)$, $\sigma_\varphi^{I}(r=a)=\sigma_\varphi^{II}(r=a)$, $\sigma_z^{I}(r=a)=\sigma_z^{II}(r=a)$, $\sigma_r^{II}(r=b_1)=\sigma_r^{III}(r=b_1)$, $\sigma_\varphi^{II}(r=b_1)=\sigma_\varphi^{III}(r=b_1)$, $\sigma_z^{II}(r=b_1)=\sigma_z^{III}(r=b_1)$, $\sigma_r^{III}(r=b_2)=\sigma_r^{IV}(r=b_2)$, $\sigma_\varphi^{III}(r=b_2)=\sigma_\varphi^{IV}(r=b_2)$, and $\sigma_z^{III}(r=b_2)=\sigma_z^{IV}(r=b_2)$. Equations (13)-(24) will be used in Section IV under to calculate the radially varying index of refraction in different pump schemes, due to the stress-optic effect. Note that the equations as derived above for the fiber stresses could also have been obtained by use of the deviation of the temperature distribution from the average and the Airy stress potential [11].

4. Index of Refractions

Using the expressions for the radial temperature distributions, reported [8] and for the stress distributions (13)-(24), we tray now to make calculation of the radially varying radial and tangential index of refraction distributions. For comparison in different pump schemes, we prefer to cast the calculation of the induced change in the index of refraction in terms of material stresses, rather than strains. We begin by writing the changes in the indices of refraction:

$$\Delta n_{r,\varphi}^{I,II,III,IV}(r)=\Delta n_{r,\varphi}^{I,II,III,IV}-n_0=\Delta n_{\beta}^{I,II,III,IV}(r)+\Delta n_{ST,r,\varphi}^{I,II,III,IV}(r) \tag{33}$$

where

$n_0=1.45$ Linear index of refraction;

$\Delta n_{\beta}^{I,II,III,IV}(r)$ Change in index due to change in index with temperature $\left(\beta=\dfrac{\mathrm{d}n}{\mathrm{d}T}\right)$;

$\Delta n_{r,\varphi}^{I,II,III,IV}(r)$ Stress-induced index changes for the r and φ components of the electric field.

As before, the roman numerals refer to Regions I, II, III and IV. Here, we will calculate $\Delta n_{\beta}^{I,II,III,IV}(r)$ using the following equation:

$$\Delta n_{\beta}^{I,II,III,IV}(r)=\beta\left(T_{1,2,3,4}(r)-T_c\right) \tag{34}$$

For Regions I, II, III and IV, becomes

$$\Delta n_{\beta}^{I}(r)=\beta\left(T_0-\frac{Q(x)\times r^2}{4k_1}-T_c\right) \tag{35}$$

And

$$\Delta n_{\beta}^{II}(r)=\beta\left(T_1(a)+A(x)\times\ln\left(\frac{r}{a}\right)-T_c\right) \tag{36}$$

And

$$\Delta n_{\beta}^{III}(r)=\beta\left(T_2(b_1)+B(x)\times\ln\left(\frac{r}{b_1}\right)-T_c\right) \tag{37}$$

And

$$\Delta n_{\beta}^{IV}(r)=\beta\left(T_3(b_2)+C(x)\times\ln\left(\frac{r}{b_2}\right)-T_c\right) \tag{38}$$

The calculation of the stress-induced index changes $\Delta n_{ST,r,\varphi}^{I,II,III,IV}(r)$ are treated in [10]. Using

$$\Delta n_{ST,r}^{I}(r) = -\frac{n_0^3}{2}\left[B_{\perp}\left(\sigma_{\varphi}^{I}(r)+\sigma_{z}^{I}(r)\right)+B_{\parallel}\sigma_{r}^{I}(r)\right] \tag{39}$$

$$\Delta n_{ST,\varphi}^{I}(r) = -\frac{n_0^3}{2}\left[B_{\parallel}\sigma_{\varphi}^{I}(r)+B_{\perp}\left(\sigma_{z}^{I}(r)+\sigma_{r}^{I}(r)\right)\right] \tag{40}$$

$$\Delta n_{ST,r}^{II}(r) = -\frac{n_0^3}{2}\left[B_{\perp}\left(\sigma_{\varphi}^{II}(r)+\sigma_{z}^{II}(r)\right)+B_{\parallel}\sigma_{r}^{II}(r)\right] \tag{41}$$

$$\Delta n_{ST,\varphi}^{II}(r) = -\frac{n_0^3}{2}\left[B_{\perp}\left(\sigma_{\varphi}^{I}(r)+\sigma_{z}^{I}(r)\right)+B_{\parallel}\sigma_{r}^{I}(r)\right] \tag{42}$$

$$\Delta n_{ST,r}^{III}(r) = -\frac{n_0^3}{2}\left[B_{\perp}\left(\sigma_{\varphi}^{III}(r)+\sigma_{z}^{III}(r)\right)+B_{\parallel}\sigma_{r}^{III}(r)\right] \tag{43}$$

$$\Delta n_{ST,\varphi}^{III}(r) = -\frac{n_0^3}{2}\left[B_{\parallel}\sigma_{\varphi}^{III}(r)+B_{\perp}\left(\sigma_{z}^{III}(r)+\sigma_{r}^{III}(r)\right)\right] \tag{44}$$

$$\Delta n_{ST,r}^{IV}(r) = -\frac{n_0^3}{2}\left[B_{\perp}\left(\sigma_{\varphi}^{IV}(r)+\sigma_{z}^{IV}(r)\right)+B_{\parallel}\sigma_{r}^{IV}(r)\right] \tag{45}$$

$$\Delta n_{ST,\varphi}^{IV}(r) = -\frac{n_0^3}{2}\left[B_{\parallel}\sigma_{\varphi}^{IV}(r)+B_{\perp}\left(\sigma_{z}^{IV}(r)+\sigma_{r}^{IV}(r)\right)\right] \tag{46}$$

where $B_{\parallel}$ and $B_{\perp}$ are the parallel and perpendicular stress-optic coefficients. Their values are $4.5\times10^{-8}\ \mathrm{cm^2/kg}$, $27.7\times10^{-8}\ \mathrm{cm^2/kg}$ respectively [11]. The numerical values of E and ν are $E = 73\ \mathrm{GPa} = 7.45\ \mathrm{kg/cm^2}$ and $\nu = 0.16$ [12].

$$\Delta n_{r}^{I}(r) = \beta\left(T_0 - \frac{Q(x)\times r^2}{4k_1} - T_c\right) - \frac{n_0^3}{2}\left[B_{\perp}\left(\sigma_{\varphi}^{I}(r)+\sigma_{z}^{I}(r)\right)+B_{\parallel}\sigma_{r}^{I}(r)\right] \tag{47}$$

$$\Delta n_{\varphi}^{I}(r) = \beta\left(T_0 - \frac{Q(x)\times r^2}{4k_1} - T_c\right) - \frac{n_0^3}{2}\left[B_{\parallel}\sigma_{\varphi}^{I}(r)+B_{\perp}\left(\sigma_{z}^{I}(r)+\sigma_{r}^{I}(r)\right)\right] \tag{48}$$

$$\Delta n_{r}^{II}(r) = \beta\left(T_1(a) + A(x)\times\ln\left(\frac{r}{a}\right) - T_c\right) - \frac{n_0^3}{2}\left[B_{\perp}\left(\sigma_{\varphi}^{II}(r)+\sigma_{z}^{II}(r)\right)+B_{\parallel}\sigma_{r}^{II}(r)\right] \tag{49}$$

$$\Delta n_{\varphi}^{II}(r) = \beta\left(T_1(a) + A(x)\times\ln\left(\frac{r}{a}\right) - T_c\right) - \frac{n_0^3}{2}\left[B_{\parallel}\sigma_{\varphi}^{II}(r)+B_{\perp}\left(\sigma_{r}^{II}(r)+\sigma_{z}^{II}(r)\right)\right] \tag{50}$$

$$\Delta n_{r}^{III}(r) = \beta\left(T_2(b_1) + B(x)\times\ln\left(\frac{r}{b_1}\right) - T_c\right) - \frac{n_0^3}{2}\left[B_{\perp}\left(\sigma_{\varphi}^{III}(r)+\sigma_{z}^{III}(r)\right)+B_{\parallel}\sigma_{r}^{III}(r)\right] \tag{51}$$

$$\Delta n_{\varphi}^{III}(r) = \beta\left(T_2(b_1) + B(x)\times\ln\left(\frac{r}{b_1}\right) - T_c\right) - \frac{n_0^3}{2}\left[B_{\parallel}\sigma_{\varphi}^{III}(r)+B_{\perp}\left(\sigma_{z}^{III}(r)+\sigma_{r}^{III}(r)\right)\right] \tag{52}$$

$$\Delta n_{r}^{IV}(r) = \beta\left(T_3(b_2) + C(x)\times\ln\left(\frac{r}{b_2}\right) - T_c\right) - \frac{n_0^3}{2}\left[B_{\perp}\left(\sigma_{\varphi}^{IV}(r)+\sigma_{z}^{IV}(r)\right)+B_{\parallel}\sigma_{r}^{IV}(r)\right] \tag{53}$$

$$\Delta n_{\varphi}^{IV}(r) = \beta\left(T_3(b_2) + C(x)\times\ln\left(\frac{r}{b_2}\right) - T_c\right) - \frac{n_0^3}{2}\left[B_{\parallel}\sigma_{\varphi}^{IV}(r)+B_{\perp}\left(\sigma_{z}^{IV}(r)+\sigma_{r}^{IV}(r)\right)\right] \tag{54}$$

We can also define the brief ringence $\Delta n_B^{I,II,III,IV}(r)$, given by

$$\Delta n_B^{I,II,III,IV}(r) = \Delta n_r^{I,II,III,IV}(r) - \Delta n_\varphi^{I,II,III,IV}(r) \tag{55}$$

Which may be calculated by using, yielding

$$\Delta n_B^{I}(r) = \frac{n_0^3}{2} B\left(\sigma_r^{I}(r) - \sigma_\varphi^{I}(r)\right) \tag{56}$$

$$\Delta n_B^{II}(r) = \frac{n_0^3}{2} B\left(\sigma_r^{II}(r) - \sigma_\varphi^{II}(r)\right) \tag{57}$$

$$\Delta n_B^{III}(r) = \frac{n_0^3}{2} B\left(\sigma_r^{III}(r) - \sigma_\varphi^{III}(r)\right) \tag{58}$$

$$\Delta n_B^{IV}(r) = \frac{n_0^3}{2} B\left(\sigma_r^{IV}(r) - \sigma_\varphi^{IV}(r)\right) \tag{59}$$

Equations (56)-(59) show that the fiber birefringence depends only on the thermally induced stresses. Finally, by using (43)-(50) and substituting (13)-(20) for the radial, tangential, and z stress components, we arrive at the final equations describing the radially varying indices of refraction in a fiber.

Where $\Delta n_r^I(r)$ and $\Delta n_\varphi^I(r)$, apart from a constant term, vary quadratically with the fiber radius, in agreement with previously published work on bulk rod laser amplifiers [13] [14]. For Region II, however, it is noted that $\Delta n_r^{II}(r)$ and $\Delta n_\varphi^{II}(r)$ vary in a complicated way that involves both a logarithmic function and an inverse square.

5. Discussions

For simplicity, we concentrated in this work on Yb^{3+}. The core region is surrounded by a circle inner cladding region with dimensions of radius 125 μm, the width of air-clad is 5 μm and which is in turn surrounded by a polymeric outer cladding region with outside diameter of about 300 μm.

5.1. Stress Effect

In **Figures 3(a)-(e)**, we plotted the stress components radial, tangential and longitudinal as a function of the radial coordinate r in different pump schemes for a Yb^{3+} fiber with a pump of 200 W, b = 300 μm is the outer radius, convective coefficient h = 40.9 W/cm·K. The quantities $B_\perp$ and $B_\parallel$ are known in the optics and laser literature as the perpendicular and parallel stress-optic coefficients their values are found in Section 4, the thermal expansion coefficient is $\alpha = 0.51\times10^{-6}/\text{k}$ [15], we show no difference between (a) and (b) in side of the pumping (left side). Moreover, a small difference in other side (side right), we show the same thing for (c) and (d) figures. However, in **Figure 3(e)** the value of stress is smaller than the previous cases. The difference between the maximum and minimum values of stress components, in the four previous cases (a, b, c, d) is in the order $2\times10^{-6}\ \text{kg}/\text{m}^2$ but in bi-directional pump scheme **Figure 3(e)** the value is the order $1\times10^{-6}\ \text{kg}/\text{m}^2$. Therefore in bi-directional pump scheme the effects of the stress is negligible with regard to the others cases.

For more clarification, we plotted the stress components as a function of the radius in different pump schemes. In **Figures 4(a)-(e)**, we observe that there is a rapid increase in air-clad region of the components radial $\sigma_r(r)$ and longitudinal $\sigma_z(r)$. However, concerning the tangential component $\sigma_\varphi(r)$, the increase is less rapid. We notice that the required boundary conditions are all satisfied. At $r = b$, the tangential $\sigma_\varphi(r)$ and longitudinal $\sigma_z(r)$ stresses are equal while the radial $\sigma_r(r)$ stress is zero along the fiber. Therefore, we anticipate that changes in the index of refraction due to the stress optic effect will be negligible in all cases of pumping and precisely in bi-directional pump scheme and thermally induced birefringence to be absent in fiber lasers.

5.2. Index of Refraction

Using (47)-(54), we plotted the tangential and the radial indices of refraction as a function of the radial coordinate r in different pump schemes, **Figures 5(a)-(e)**, the pump power used is 200 W, the fiber outside radius is b = 300 μm, and the convection coefficient is h = 40.9 W/m·K, and $\beta = 10^{-5}/\text{k}$ [12]. The curves for $\Delta n_r(r)$

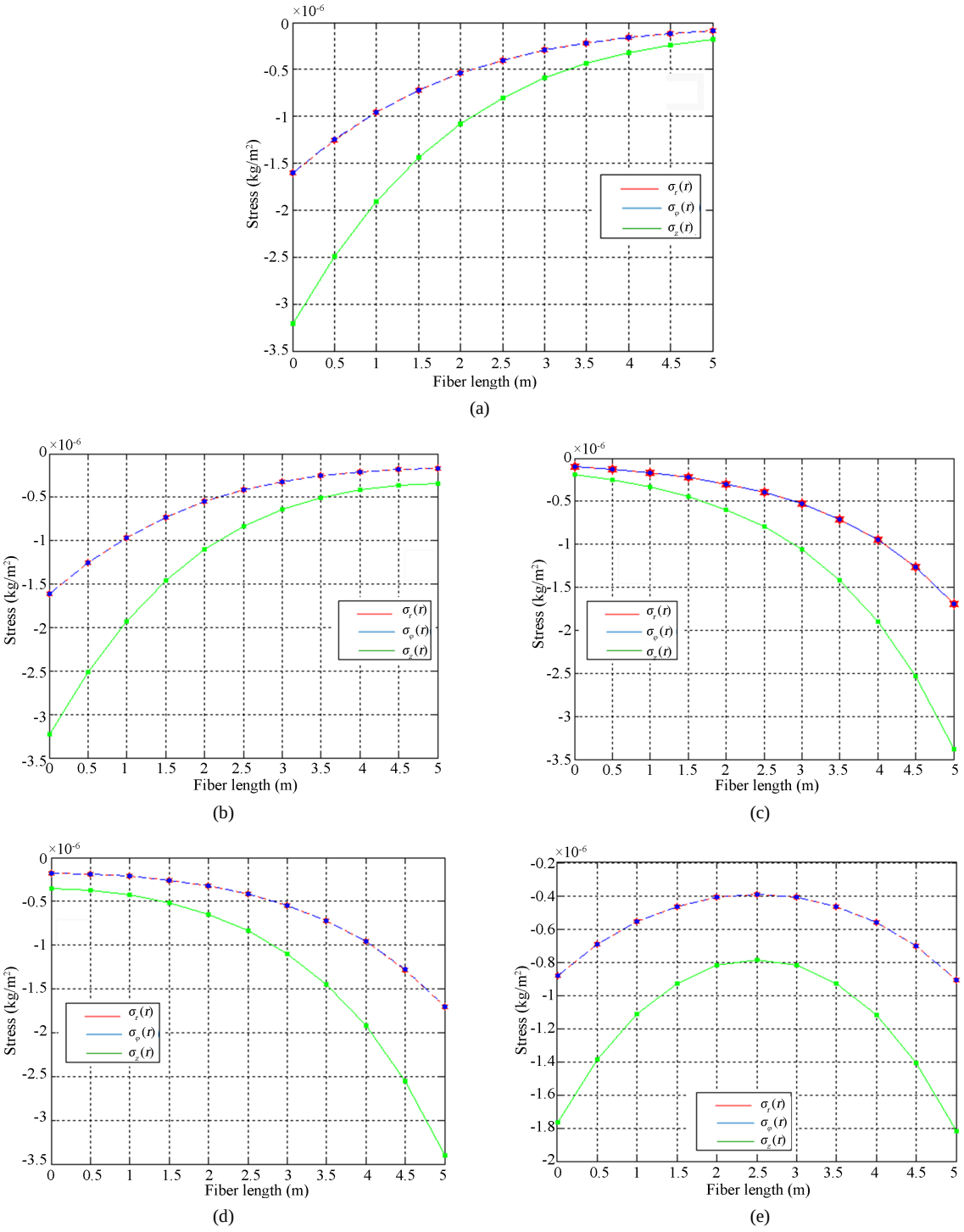

Figure 3. Distribution of longitudinal stress in PCF at 200 W pump of 940 nm load calculated by FDM analysis. (a) Forward pump schemes; (b) Forward pump with a reflectivity of 98%; (c) Backward pump schemes; (d) Backward pump with a reflectivity of 98%; (e) Tow-end pump schemes.

and $\Delta n_\varphi(r)$ are essentially identical in r = 0 μm and in r = b, and the radially varying index is due to $\beta = \frac{\mathrm{d}n}{\mathrm{d}T}$ only, because $\sigma_r(r)$ and $\sigma_\varphi(r)$ are so small. The values of the change in index of refraction de-

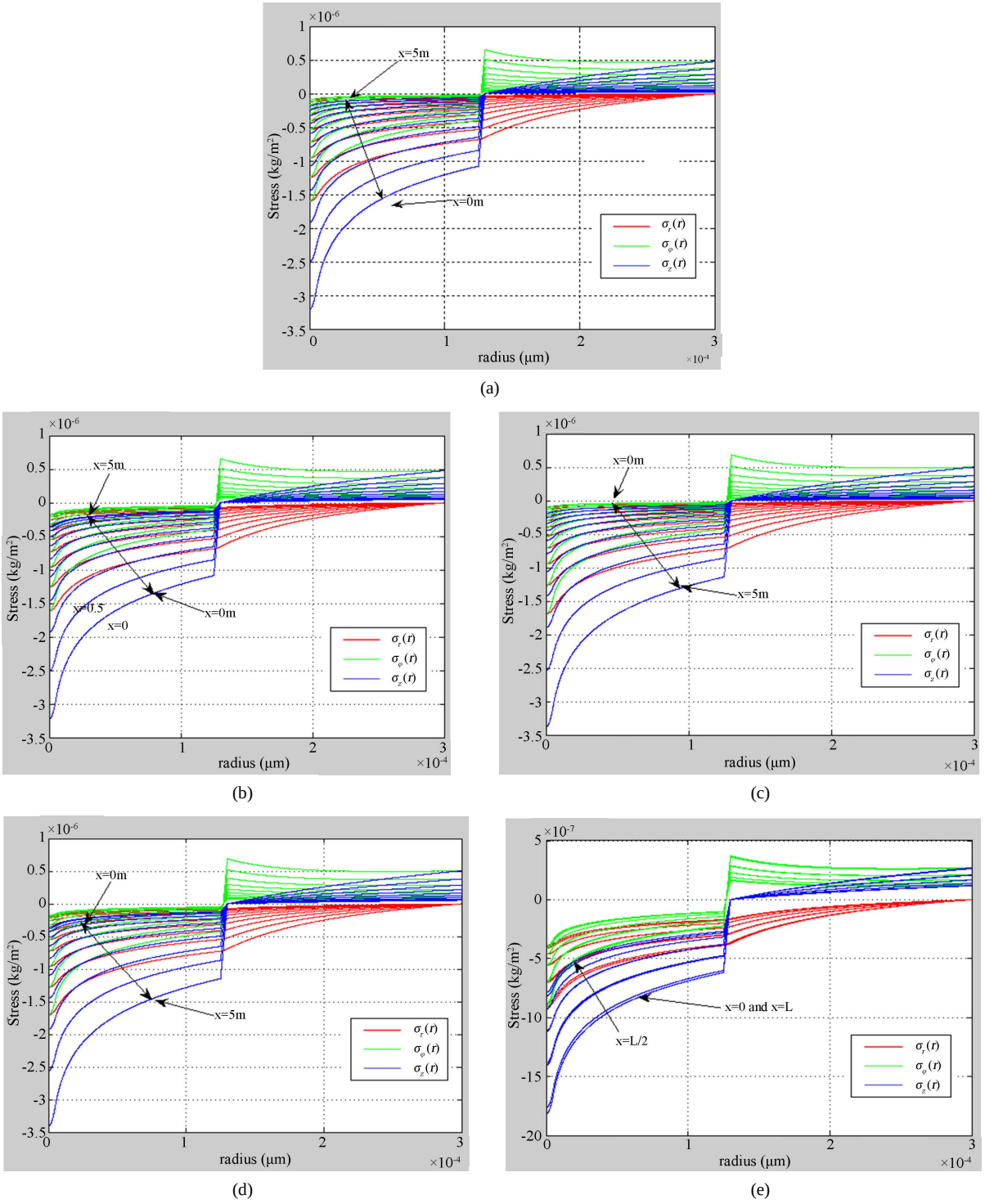

Figure 4. Distribution of radial stress in PCF at 200 W of 940 nm pump load calculated by FDM analysis. (a) Forward pump schemes; (b) Forward pump with a reflectivity of 98%; (c) Backward pump schemes; (d) Backward pump with a reflectivity of 98%; (e) Tow-end pump schemes.

crease along the fiber lasers in **Figure 5(a)** and **Figure 5(b)** from the order 1.2×10^{-3} to 0.1×10^{-3}. In **Figure 5(c)** and **Figure 5(d)** the values of change in index of refraction increase in the opposite order 0.1×10^{-3} to 1.2×10^{-3}. Nevertheless, in **Figure 5(e)** the value is in order of 3×10^{-3} to 7×10^{-3}. As result, we notice in side of

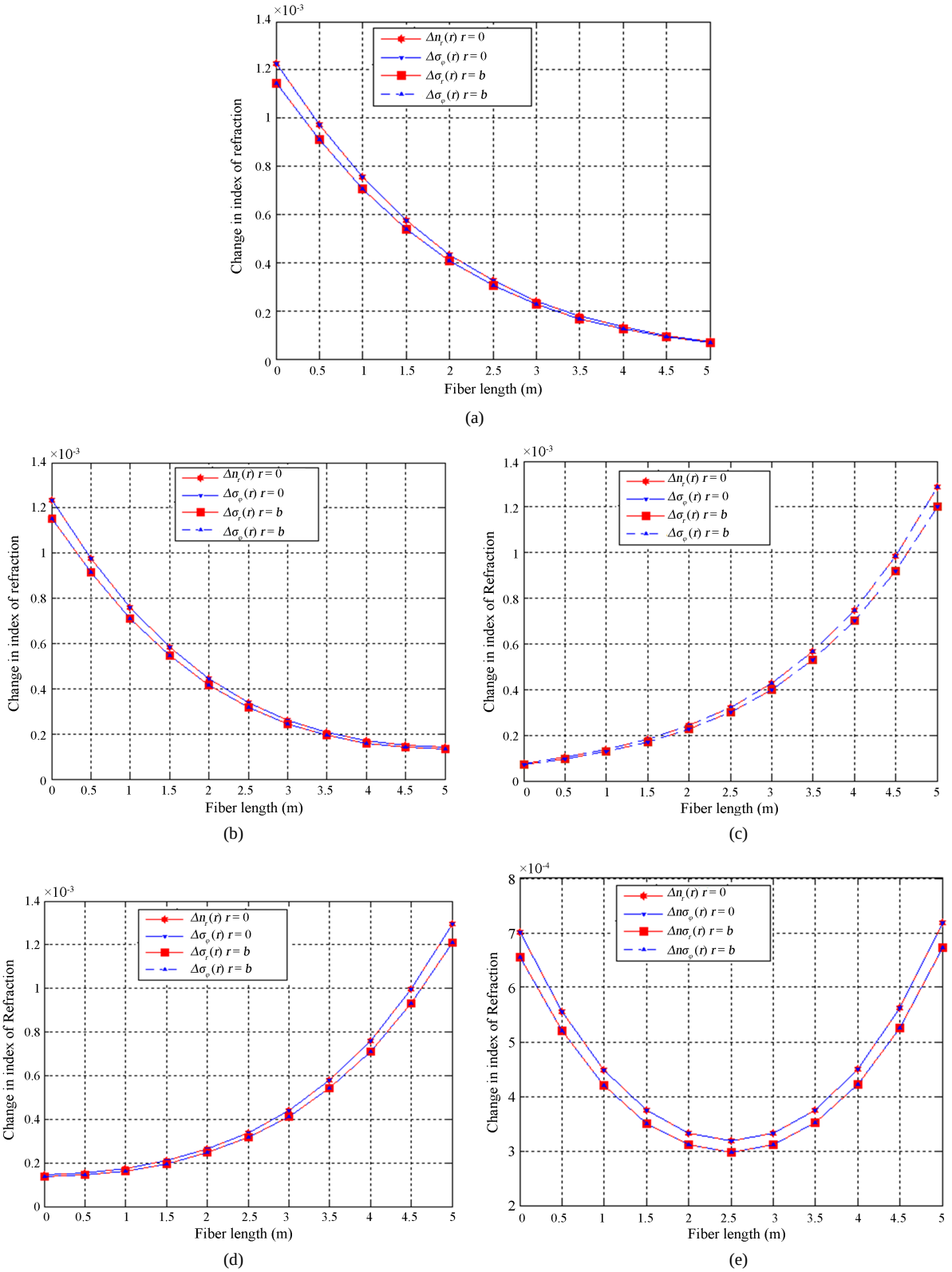

Figure 5. The change in index of refraction in PCF at 200 W pump load calculated by FDM analysis. (a) Forward pump schemes; (b) Forward pump with a reflectivity of 98%; (c) Backward pump schemes; (d) Backward pump with a reflectivity of 98%; (e) Tow-end pump schemes.

pumping there is a small difference of the change in index of refraction between the fiber core $r = 0$ and in the outer clad $r = b$, the four **Figures 5(a)-(d)**. However, in **Figure 5(e)** the difference of the change in index of refraction between the fiber core $r = 0$ and in the outer clad $r = b$ is small along the fiber.

6. Summary

In this paper, we have investigated a comparison of stress and thermo-optic of photonic crystal fiber (PCFs) in different pump schemes. Using in these calculations a simple model of (PCFs) and finite differential method (FDM), we have revealed the temperature in the core of the fiber and by laws of heat transfer, we determined its value at the surface of the fiber and the stress value in the different regions of the fiber.

In summary, regarding stress, thermo-optic and the change in index of refraction, their value does not have a great effect on the quality of the laser beam in different pump schemes, especially in the case of the bi-directional pumping. Hence, after this investigation, we proved the architecture of laser cavity that was the most convenient in specific condition. The bi-directional pump scheme is the most suitable because it has less thermal effects than the other cases. However, the backward pump with reflection of 98% and the forward pump with reflection of 98% save more energy than the backward pump with reflection of 0%, the forward pump with reflection of 0% and bi-directional pump scheme.

References

[1] Limpert, J., Liem, A., Zellmer, H. and Tunnerman, A. (2003) 500 W Continuous-Wave Fiber Laser with Excellent Beam Quality. *Electronics Letters*, **39**, 645-647. http://dx.doi.org/10.1049/el:20030447

[2] DiGiovanni, D.L. and Muendel, M.H. (1999) High Power Fiber Lasers and Amplifiers. *Optics and Photonics News*, **10**, 26-30. http://dx.doi.org/10.1364/OPN.10.1.000026

[3] Platonov, N., Gapontsev, V.P., Shkurihin, O. and Zaitsev, I. (2003) 400 W Low-Noise Single-Mode CW Ytterbium Fiber Laser with an Integrated Fiber Delivery. *Conference on Lasers and Electro-Optics*, Optical Society of America, Washington DC, 6 June 2003.

[4] Muendel, M.H. (1999) High-Power Fiber Laser Studies at the Polaroid Corporation. *Proceedings of the SPIE Conference High-Power Lasers*, San Jose, 24 June 1998, Vol. 3264, 21-29.

[5] Shang, L. (2011) Comparative Study of the Output Characteristics of Ytterbium-Doped Double-Clad Fiber Lasers with Different Pump Schemes. *Optik*, **122**, 1899-1902. http://dx.doi.org/10.1016/j.ijleo.2010.11.021

[6] Knight, J.C. and Russell, P.St.J. (2002) New Ways to Guide Light. *Science*, **296**, 276-277. http://dx.doi.org/10.1126/science.1070033

[7] Knight, J.C., Briks, T.A., Cregan, R.F., *et al.*, (1998) Large Mode Area Photonic Crystal Fiber. *Electronics Letters*, **34**, 1347-1349. http://dx.doi.org/10.1049/el:19980965

[8] Abouricha, M., Boulezhar, A. and Habiballah, N. (2013) The Comparative Study of the Temperature Distribution of Fiber Laser with Different Pump Schemes. *Open Journal of Metal*, **3**, 64-71. http://dx.doi.org/10.4236/ojmetal.2013.34010

[9] Limpert, J., Schreiber, T., Liem, A., Nolte, S. and Zellmer, H. (2003) Thermo-Optical Properties of Air-Clad Photonic Crystal Fiber Lasers in High Power Operation. *Optics Express*, **11**, 2982-2990.

[10] Boley, B.A. and Weiner, J.H. (1985) Theory of Thermal Stresses. Kreiger, Melbourne.

[11] Brown, D.C. and Hoffman, H.J., IEEE Member (2001) Thermal, Stress, and Thermo-Optic Effects in High Average Power Double-Clad Silica Fiber Lasers. *IEEE Journal of Quantum Electronics*, **37**, 207-217.

[12] Bass, M., Ed. (1995) Handbook of Optics (Sponsored by the Optical Society of America). Vol. II, Devices, Measurements, and Properties. McGraw-Hill, New York.

[13] Eggleston, J.M., Kane, T.J., Kuhn, K., Unternahrer, J. and Byer, R.L. (1984) The Slab Geometry Laser—Part I: Theory. *The IEEE Journal of Quantum Electronics*, **QE-20**, 289-301. http://dx.doi.org/10.1109/JQE.1984.1072386

[14] Brown, D.C. (1998) Nonlinear Thermal Distortion in YAG Rod Amplifiers. *IEEE Journal of Quantum Electronics*, **34**, 2383-2382. http://dx.doi.org/10.1109/3.736113

[15] Krupke, W.F., Shinn, M.D., Marion, J.E., Caird, J.A. and Stokowski, S.E. (1986) Spectroscopic, Optical, and Thermomechanical Properties of Neodymium- and Chromium-Doped Gadolinium Scandium Gallium Garnet. *Journal of the Optical Society of America B*, **3**, 102, 113.

Scientific Research Publishing (SCIRP) is one of the largest Open Access journal publishers. It is currently publishing more than 200 open access, online, peer-reviewed journals covering a wide range of academic disciplines. SCIRP serves the worldwide academic communities and contributes to the progress and application of science with its publication.

Other selected journals from SCIRP are listed as below. Submit your manuscript to us via either submit@scirp.org or Online Submission Portal.